KLOE Note N. 97

March 13, 1994

Measurement of the space point resolution of the drift chamber prototypes

Riccardo de Sangro

Abstract

We have tested two small drift chambers with different square cell configurations in a test beam of energies between 150 and 350 MeV with various helium based gas mixtures. In this work we show that a resolution of $\leq 200\mu m$ can be achieved with a 90% He - 10% iC_4H_{10} gas mixture.

1. Introduction

In this paper we report on the tests that have been made to get an experimental confirmation of the practical possibility to achieve some of the goal performances of the KLOE drift chamber. A more detailed discussion of the physics motivations for the required performances and the design solutions adopted to obtain them can be found in refs.[1] [2] . In the following we will just briefly mentions the aspects more relevant to this work.

The main design goals are a resolution on transverse momentum of ~0.3%, which is based on assuming ~200μm for the point resolution in the transverse plane, and a high ($\geq$ 98%) tracking reconstruction efficiency for the CP violating decay $K_L \rightarrow \pi^+\pi^-$. Both of them depends on the drift gas chosen and on the geometry of the cell.

The low (~150-250 MeV/c) particle momenta involved in the decays of interest, result in the multiple Coulomb scattering being the dominating contribution to the momentum resolution, which compels one to use the lightest possible materials throughout the chamber. The transparency of the chamber is also needed to preserve the high detection efficiency for low energy photons in the electromagnetic calorimeter outside it, which is needed to detect the neutrals. Widespread use of special materials such as carbon fibers, characterized by their strength and low radiation length, is therefore foreseen for the construction of the mechanical structure of the chamber. Also, the number of sense and field wires will have to be kept to a minimum, and very light, helium based drift gas mixtures are under study.

Since the charged tracks from the decays of can originate anywhere inside the chamber volume and leave in all directions, an interaction region pointing geometry is not the most efficient and thus the whole chamber volume will be uniformly filled with closely packed cells.

The z coordinate measurement along the wires is done with stereo layers. In the present design, the chamber will have all layers stereo, alternating positive and negative angles. To realize such a layout and to minimize the number of wires per cell, a square cell has been adopted.

To test both the cell geometry and the relatively little known gas mixtures, we have built two small drift chamber prototypes with square cells: *Prototype 0.1* with a 3:1 ratio of field to sense wires, and *Prototype 0.2* with a ratio of 2:1 (see fig. 1.1).

They are both made of an array of 7x7 square cells about 2 cm wide, differing between them only for the fact that *Prototype 0.1* has one more wire on each of the vertical sides of the squares. Table 1lists the principal characteristics of the two devices.

Table 1. Prototypes main characteristics.

Wire length	50 cm
Wire diameter	sense: $20\mu m$/ field: $80\mu m$
Wire material	sense: Cu-Be / field: Al
Cell shape/size	square/ $(2x2)cm^2$
Field to sense wire ratio	Prot 0.1 : 3:1 – Prot 0.2 : 2:1

In fig. 1.2the layout of the cells is shown and in fig. 1.3the details of the two cells showing the differences between the two geometries.

Only the innermost 5x5=25 sense wires are instrumented, while the outer ones are set at the proper high voltage only to reduce the distortion of the electric field in the cells under study. All the field wires are grounded. The signals from the wires are amplified by a transresistance amplifier developed in Frascati as a first prototype of the final front-end read out for the final chamber.[3]

2. Test Beam Setup

The two prototypes have been exposed to a particle beam (mostly pions) of energies between 150 and 350 MeV made available in the $\pi\mu3$ experimental area of PSI.[4] A sketch of the experimental setup is shown in fig. 2.4.

The beam entered from the right first traversing the (4x4) cm^2 scintillator S1, then the first of two multiwire proportional chambers, MWPC 1 and MWPC 2, positioned immediately before and after the two prototypes *Prototype 0.1* and *Prototype 0.2* . A second (12x12) cm^2 scintillator S2 followed MWPC 2.

The prototypes were sitting vertically (wires running vertically) on two revolving supports that enabled us to rotate them about their axis and study their response to different incident beam angles.

The MWPCs are made of two orthogonal planes of 128 wires with a 1 mm pitch. The signals above a set threshold constituted a digital hit; adjacent hit wires were then grouped in clusters. After this operation one was left with a cluster list with the coordinates of the clusters for each plane, which was written to disk. The resolution on the position thus obtained is expected to be $\sim 300\mu m$.

The two MWPCs therefore gave two position measurements of the incident tracks, one for each of the two projection planes X,Y and X,Z as defined in the reference system chosen for the analysis and shown in fig. 2.4. From these measurements we could determine the incident particles straight trajectories in the prototypes.

The coincidence S1*S2 of the two scintillators formed a trigger. The CAMAC acquired signals included one TDC and one ADC value for each sense wire (100 channels), the MWPC latches (128x4 channels), two ADC value for the scintillators plus a number of scaler channels with various rates. Also, the time of flight of the beam particles going from the production target to the setup was acquired in order to get some information on the type of beam particle (π , μ , e, p etc.).[5]

The CAMAC was read out with a PC running an acquisition software developed at PSI and the data stored on a μVAX disk connected to the PC. The program allowed on line histogramming of the acquired data for monitoring, and performed the clustering of the MWPC hits. The data was then transferred to tape for the off-line analysis. In fig. 2.5an event is shown; the solid line represents the external track, the others represent the tracks fitted with the two prototypes individually and the track obtained with a combined fit of the two. A profile of the beam and a measure of its angular dispersion as measure in the MWPCs is shown in fig. 2.6.

3. Data Analysis

The test beam data has been collected in two one-week periods in June and July of 1993. Different runs have been taken with different combinations of gas mixture, beam incidence angle and operating voltage of the chambers. The different mixtures tested included 90% He - 10% iC_4H_{10} , 95% He - 5% iC_4H_{10} , 60% He - 40% CH_4 , 80% He - 20% CO_2 and 60% Ar - 40% iC_4H_{10} .

In this paper we report on the data taken with 90% He - 10% iC_4H_{10} , a summary of which is given in Table 2.

Table 2. Summary of the data runs used in the present analysis

RUN #	Φ angle (degrees) Proto 0.1	Proto 0.2	All Runs:
513	0	0	Gas mixture 90% He - 10% iC_4H_{10}
519	0	90	Beam Energy: 250 MeV
520	0	60	HV Proto 0.1: 1800 V
522	30	30	HV Proto 0.2: 1950 V
523	60	0	
525	90	0	

3.1 Track Fit

The main scope of this analysis is to study how well could one reconstruct the beam particles trajectories inside the chambers, and more precisely with what spatial resolution one could measure the impact parameters of *real* tracks inside the cells.

To do this one needs to first determine which wires were hit by the particle, then apply some function to translate the time measurements to a distance, and finally perform a fit with these points to a straight line. The residuals of this fit give an estimate of this resolution.

Hit Selection

The first selection criterium applied to the data to look for events with a good track, was to ask for a MWPCs track, being it defined as two one-cluster hits in each of the two MWPCs Y projections. These points give the *external track*'s parameters. This requirement already cuts about 40% of the events, due to a somewhat low MWPCs efficiency (~80% each).

In the events selected, the external track is used to determine which cells had been traversed by the particle. Its distance of closest approach to all the cells with a TDC reading in range is calculated, and compared to the R_d obtained from the time measurement of the cells. All the hits in which the two differed by more than 1.2 cell radii are discarded. The ADC reading of all the others are then required to be 3σabove the pedestals.

For all the events in which there are at least 4 hits in each prototype, a fit is attempted.

Fit Procedure

Since the time measurements can only be translated in radial distances from the wires and not to single points in space x_i, y_i, the fit is done by looking for straight lines which are simultaneously tangent to all the circles centered in the positions of the hit wires, and with radii proportional to the drift times via the space-to-time relation.

Both parameters of the fitting line are varied and the distances of closest approach ρ_i to all the fitted cells calculated at each iteration. The fit is required to minimize the χ^2 :

$$\chi^2 = \sum_i \frac{(\rho_i^M - \rho_i)^2}{\sigma_i^2}$$

where the ρ_i^M are the measured starting values, and σ_i are the errors of each cell, which are expected to be a function of the distance from the wires. The error function used is shown in fig. 3.7. A difficulty inherent to this position measurement is that of left-right ambiguities: the time gives only the distance from the wire but not the *direction* the ionization is coming from. Such ambiguities are resolved by the fit most of the times because the cells are slightly staggered, but there still remain some cases in which the fit results in a bad track giving a good χ^2 .

We have tried to resolve this problem using the information of the external track to decide which side of the wire a particular track had crossed. It turns out that is very difficult to implement such a thing in our 'circles' fit. We have therefore also tried a simple least square fit to a straight line, in which the x_i were fixed to the nominal coordinates of the wires and the y_i were the y nominal coordinates of the wires $\pm$ the measured drift distances, where the sign was chosen based on where the external track was. The error in fixing the x_i's is not significant because the tracks are almost horizontal, thus the point of closest approach has a coordinate which is indeed $X_{doca} \sim X_{wire}$.

Althoug we have indeed seen a slight improvment in the χ^2 distribution with this linear fit, we have decided not to rely too much on the extra information given by the external tracking in order not to obtain results that may turn out to be too optimistic, and decided to use only the 'circles' fit.

It is worth noting at this point that the external tracking has in fact been used in the track fit only to select the 'good' hits, and only because we did not want to spend any time with the pattern recognition of beam tracks.

It is important to notice that to apply this procedure one has to know the space to time relation to a very good precision, as well as the relative position of the chambers, MWPCs etc.

3.2 Set-up Alignment

So the first thing to do to obtain a good time to distance relation is to check the relative alignment between the MWPCs and the prototypes.

The origin of the reference system is chosen to be exactly in the middle of the two prototypes in X, and in the center of the MWPCs active region in Y. The relative Y offset between the two MWPCs was measured to be zero in a survey of the setup, as was expected given the precision of their mechanical assembly. Note that any small deviation from the nominal value of the X coordinate of either the MWPCs and/or the prototypes, produces a negligible effect on the determination of the position of the tracks relative to the wires, because the tracks are almost horizontal, i.e. aligned with X.

The MWPCs are therefore aligned in Y and what we need to do is only to find the position of the two prototypes with respect to them. Starting from the nominal positions of each prototype obtained with the survey measurements, the small deviations from them can be reduced to a rotation about their vertical axis and an offset in their Y coordinate.

These deviations were measured by comparing, event by event, the offset and angular coefficients of the external track with those of the two tracks independently fitted starting from the prototypes hit cells.† A systematic shift from zero in the distribution of the difference between the angular coefficients indicates a rotation in the XY plane of the prototype with respect to the chambers. After correcting for it, we repeated the fit and then plotted the difference between the Y coordinate extrapolated from the external track in a given cell and that extrapolated in the same cell from the prototype fitted track. Again, a shift in this distribution indicates a systematic offset of the prototype with respect to its nominal position. That this is a real overall displacement of the whole prototype is confirmed by the fact that the same offset is simultaneously observed in different cells in the prototype. In fig. 3.8we show these distributions. The procedure has been repeated for both prototypes independently and for all of the analyzed runs.

3.3 Space to Time Relations

The time-to-distance relation is the relation between the measured time of arrival of the ionization signal on the prototypes wires (that is the drift time, t_d) and the position where the ionization was produced by the particle inside the corresponding cell. If one knows the real distance of closest approach to the wire (R_d) of the track, this can be

† A 0^{th} order space-to-time relation can be obtained before any alignment is made, and used to perform a first track fit in the prototypes.

done relatively easily by correlating the drift time t_d to the known R_d , and then fitting a function which will give the distance corresponding to each measured time.

In our setup, the real R_d was obtained by using the particle track trajectory measured with the MWPCs, which we have already called *external track* because is determined independently from the prototypes.

After all the position corrections have been applied, the fits to the space to time functions have been repeated. In fig. 3.9the t_d Vs R_d correlation is shown for a cell of the two prototypes for ϕ=0° and 90° . The sign of R_d has been assigned based on whether the tracks passed above the wire ($Y_{trk} \geq Y_{wire}$, $R_d \geq 0$) or below it ($Y_{trk} \leq Y_{wire}$, $R_d \leq 0$). From the 0° plots one can clearly see the effect of the missing field wire on the sides cell structure of *Prototype 0.2* , namely the lengthening of the drift time of the 2:1 with respect to the 3:1 cell near the border, which is due to its lower electric field in this region. They also show that tracks entering the 2:1 cell at 90° see a cell very similar to the 3:1, and that the latter is identical for tracks at 0° or 90° as expected.

To perform the fit, a profile histogram was obtained from these scatter plots. This is shown superimposed to the scatter plot before (fig. 3.10b) and after (fig. 3.10c) applying the cuts shown in fig. 3.10a aimed at removing some of the background noise; fig. 3.10d shows the comparison of the two profiles. As it is apparent from these plots, without the cuts the profile histogram does not adequately reproduce the shape of the scatter plot neither very close to the wire nor closer to the cell border.

The function used to fit the profile is the parabola:

$$t_d = AR_d^2 + B|R_d| + t_0$$

where the parameter t_0 takes into account any small errors in the evaluation of the TDC pedestals which are due to the unavoidable delay of the signals in the cables, electronics etc. These pedestals are estimated for every cell by looking at the beginning of the raw TDC time distributions, then subtracted from the raw TDC reading before the conversion to ns. Inverting this function one gets the drift distance for any measured t_d .

The correct choice of t_0 is very important because it affect the track fit near the wires, and at the same time is difficult because there are many effects to take into account when the track get close to the wire.

Firstly, even at zero impact parameter the time of arrival of the first cluster is not always zero, but on the average is $\lambda/2$, if λ is the mean distance between ionization clusters, divided by the drift velocity. This is due to the very low ionization density of the gas mixture, and the effect becomes negligible very soon going away from the wire (see fig. 3.11). This effect can and has been corrected for.

A second effect is due to the finite resolution in the extrapolation of the tracks position in the cells, which is due to a combination of multiple Coulomb scattering of the beam particles in air and other materials and the MWPCs resolution, and amounts to $\sim 600\mu m$. Given the fact that the time measurements cannot fluctuate to values below a minimum (which is the starting point of the time spectrum) when we take the average time of those tracks whose position extrapolates to a very small distance from the wire, we get a number that remains greater than zero, even when the distance is zero. This situation is very clear by looking at the t_d Vs R_d correlation plots in the proximity of $R_d = 0$, where the profile histogram obtained by doing such an average is clearly away from $t_d = 0$.

At this point there are two possible approaches: either one fixes t_0 to the value corresponding to the beginning of the spectrum (which after all is the *real* t_0, because the TDC measured a zero drift time), or one fit the t_0. In the first case the space-to-time relation is not reproduced very well, especially near the wire, but the gas parameters like the drift velocity at the wire (which is directly given by the inverse of the fitted parameter B) assume values that are in good agreement with the expectations.[6] In the second case the space-to-time relations get reproduced much better, both closer to the wire and towards the cell's border, but in this case the drift velocities at the wires turn out about a factor of two higher than expected. It is not too surprising though, given the external tracking extrapolation resolution, that we cannot measure these parameters near the wire.

If the space-to-time relation is not correct, the effect appears as a bias in the mean value of the distributions of the residuals of the track fit that depend on the distance from the wire. An example of this is shown in fig. 3.12, where a comparison is made of the two fits, labeled NEW (fitted t_0) and OLD (fixed t_0); the two cases also differ in the cuts applied to the t_d Vs R_d correlation plot before fitting. These systematic effects in the determination of the space-to-time relations make it very difficult to assign the correct error to the measurement and therefore lead to a χ^2 distribution which is not very good.

In fig. 3.13we compare the χ^2 distributions for the two cases in the two prototypes, and they both have a rather high average value. In fig. 3.14we show as an example how the average resolution for cell 8 compares for the two cases. The gaussian fits give a $\sigma$of $\sim 340\mu m$ for *Prototype 0.1* and $\sim 310\mu m$ for *Prototype 0.2*, and were made to have an idea of the size of the errors to be used in computing the χ^2. The fact that the χ^2 /dof average value is still higher than one is clearly due to the fact that the distributions are not gaussian and have rather long tails.

The space-to-time relations can in principle be corrected for, and with a few iterations it should be possible to cope with this problem. The reason why we observe a bigger improvement for *Prototype 0.2* is because the fit for *Prototype 0.1* had been already worked on several times, albeit using always the same fitting method. This improvement is also reflected in the width of the $\Delta\Phi$ distributions, as is shown in fig. 3.15. The difference in angle between the external and the fitted tracks is basically due to the measurement error in the prototypes, and its rather large size is due to the short (10 cm) lever arm of the measurement. The width of $\sim 6.6mrd$ correspond to an average cell error of $\sim 330\mu m$, that is in fair agreement with what is observed above.

3.4 Resolution Vs drift distance

It is an important point to note that this error is averaged over the whole cell and, as we have already seen, is mainly due to the systematics. By looking at the residuals as a function of R_d one can measure the resolution that could in principle be achieved once the space-to-time relations are well modeled for all R_d , and all the systematic effects have been understood and corrected for.

In fig. 3.16and fig. 3.17the plots of the residuals of the fit as a function of R_d for the two prototypes are shown. The residuals plotted for each given cell are calculated from fits which include the cell itself, and is therefore an optimistic estimate of the real resolution. For the cell of the figure, one could take $\sim 160\mu m$ as an average value throughout the cell, excluding the region very close to the wire and very far from it; this number would translate in a resolution of $\sim 190\mu m$.

The different curves are obtained for different track incidence angles, and different space-to-time relations have been used for each different angle; the resolution is very similar at all angles in both prototypes.

We have obtained similar results for other cells. In fig. 3.18and fig. 3.19we have plotted the resolution as a function of R_d for 5 different cell for each prototype. The cells are all in one column and for the run chosen, the tracks all traversed the prototypes entering from cell 23 and exiting from cell 3, at 0 incidence angle. The resolutions are very similar to those above.

4. Conclusions

We have analyzed the test beam data taken at PSI in July 1993, measured the time-to distance relations in each prototype and reconstructed the beam tracks in the prototypes. This analysis has shown that the design goal resolution of $\leq 200\mu m$ can be achieved in both cell configurations 3:1 and 2:1.

A comparison of runs taken at different beam incidence angles has not shown any dependence of the resolution on such angle in either of the prototypes.

Within the present measurement errors, we observe no significant difference in the resolution of the two cell types in any of the situations analised.

The main sources of error are the systematic effects due to the imprecise knowledge of the space-to-time relations, which is in turn due to the error in the tracks extrapolation inside the prototypes. We have no reason to believe that these effects could not be eliminated in the future, with an improved external tracking, or even in the present data by applying some iterative correction procedure.

REFERENCES

1. "The KLOE detector technical proposal", The KLOE Collaboration, LNF-93-002 (IR); January 1993.
2. "Proposal for a ϕ-Factory", The ϕ-factory study group, LNF-90/031(R); April 1990.
3. G.Felici *et al.*, "Front end chamber electronics status report". KLOE Note N.66, Oct 1993.
4. Paul Scherrer Institute, now become Inst. for Intermediate Energy Physics of ETH, Villigen, Zurich, Switzerland.
5. M.Pollack, "Energy loss measurement in Prototype 0.1", KLOE Note N.85, Jan 1994.
6. See the discussion in G.Finocchiaro, KLOE Note N.92, March 1994 and references therein.

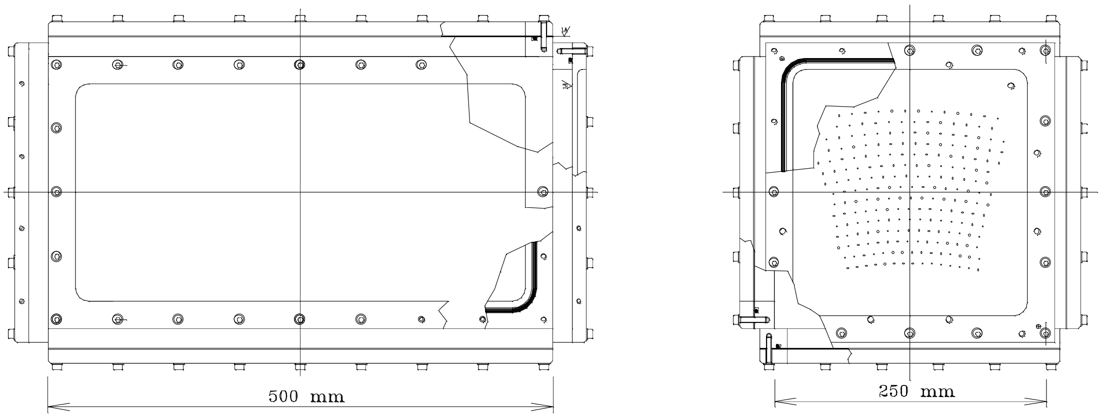

Figure 1. Mechanical skecth of the prototype chambers built.

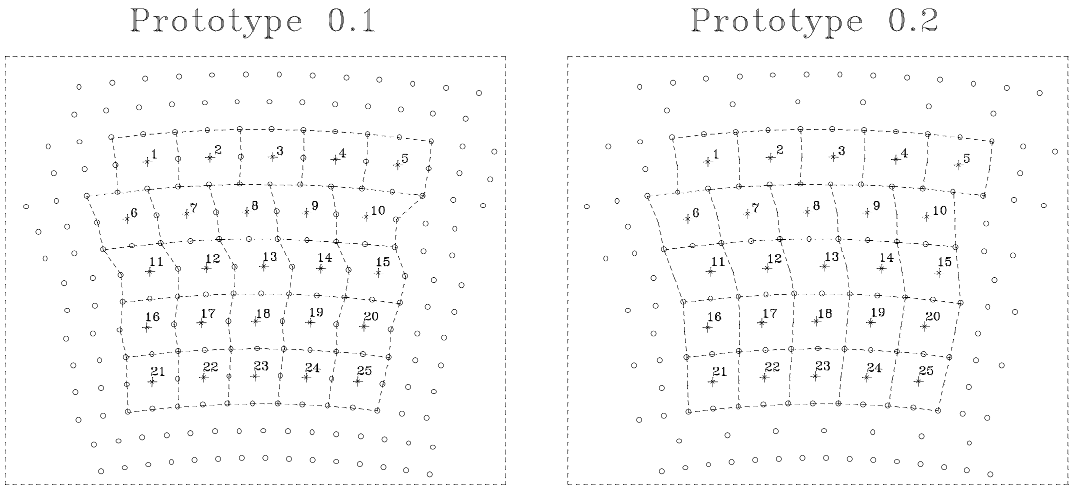

Figure 2. Cells layout in the two prototypes.

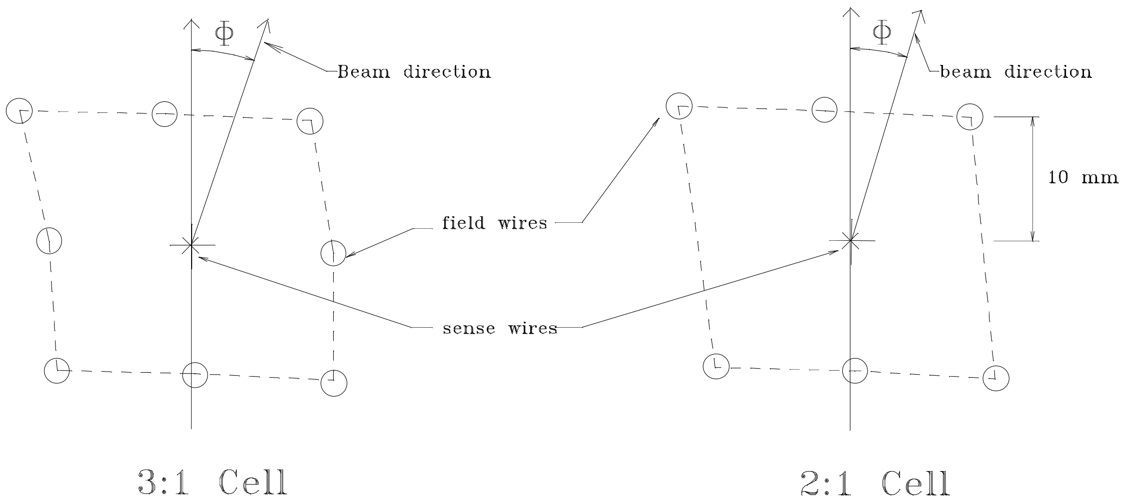

Figure 3. Detail of the two cells.

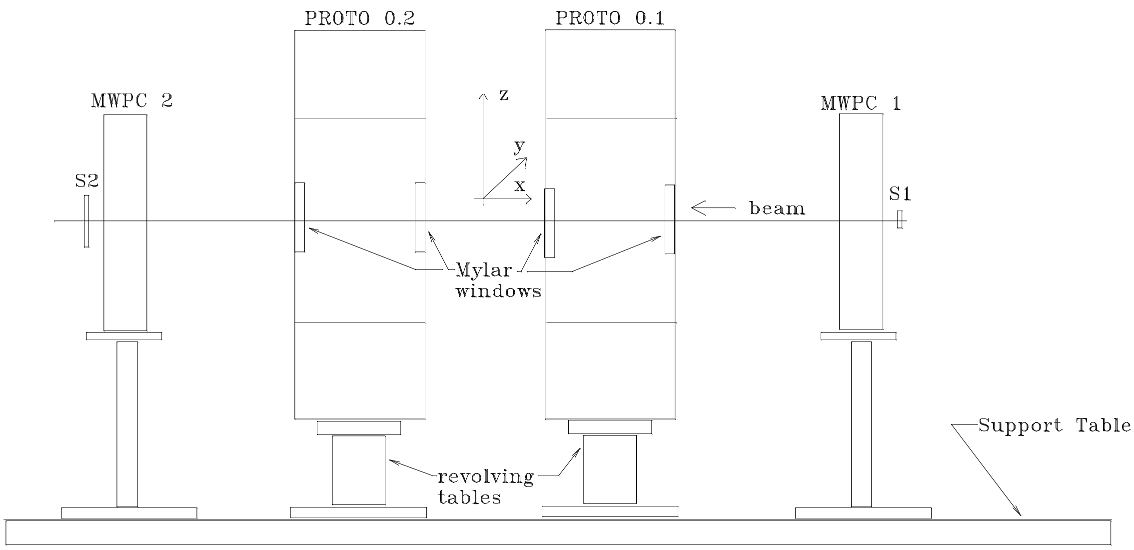

Figure 4. Sketch of the experimental setup at PSI. The coordinate system used in the analysis is also shown.

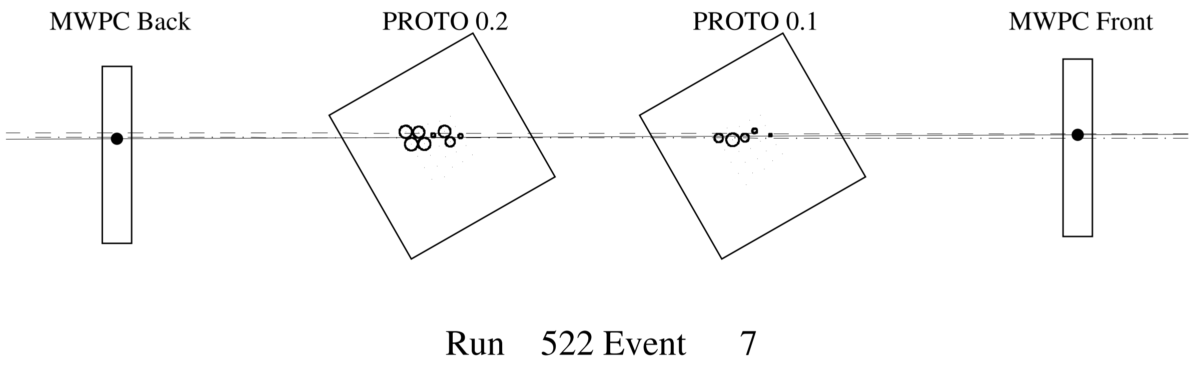

Figure 5. Display of one event of a run taken at $\Phi = 30^\circ$. The solid line is the external track, the other lines represent the fit done with the prototypes.

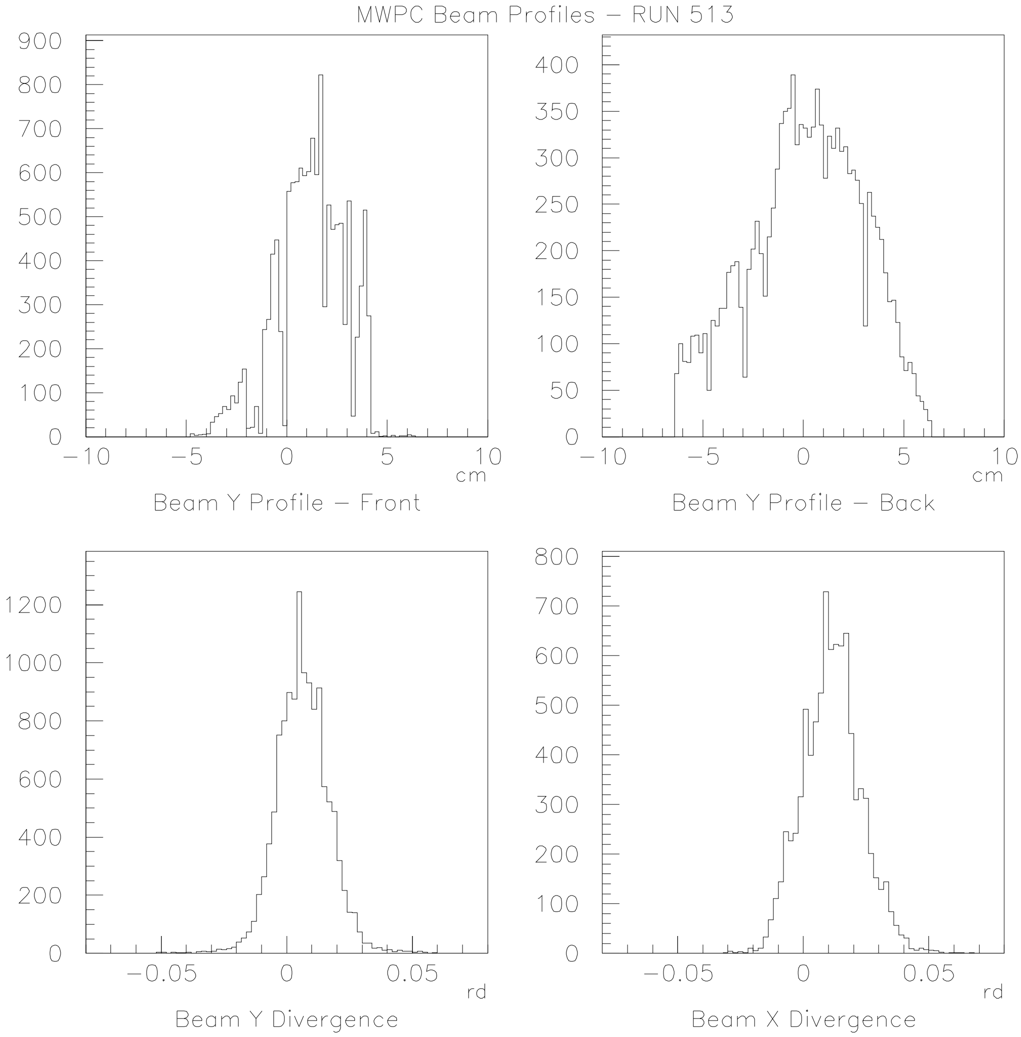

Figure 6. Beam profile obtained with the MWPCs. The X and Y width of the profiles reflect the sizes of the scintillators S1 and S2.

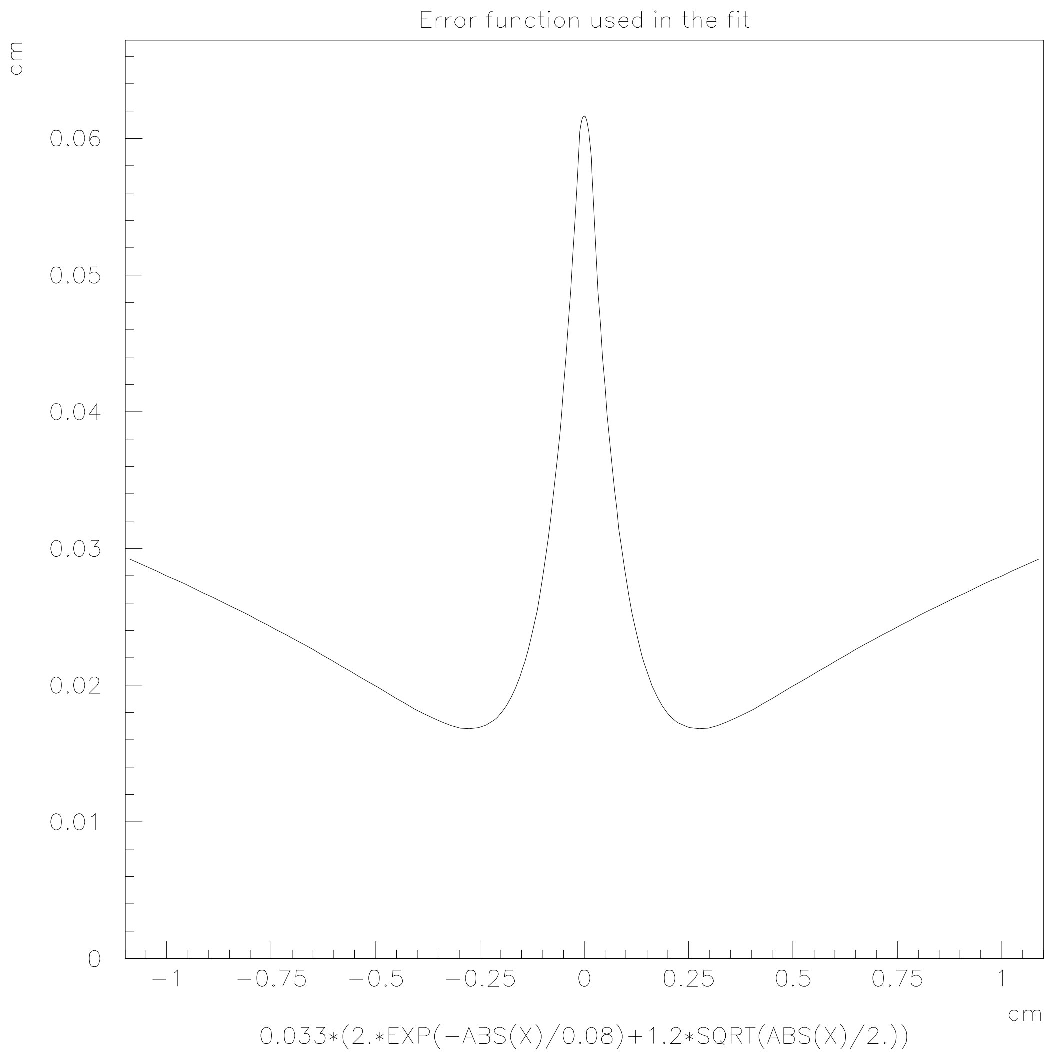

Figure 7. Function used to represent the point measurement error as a function of R_d .

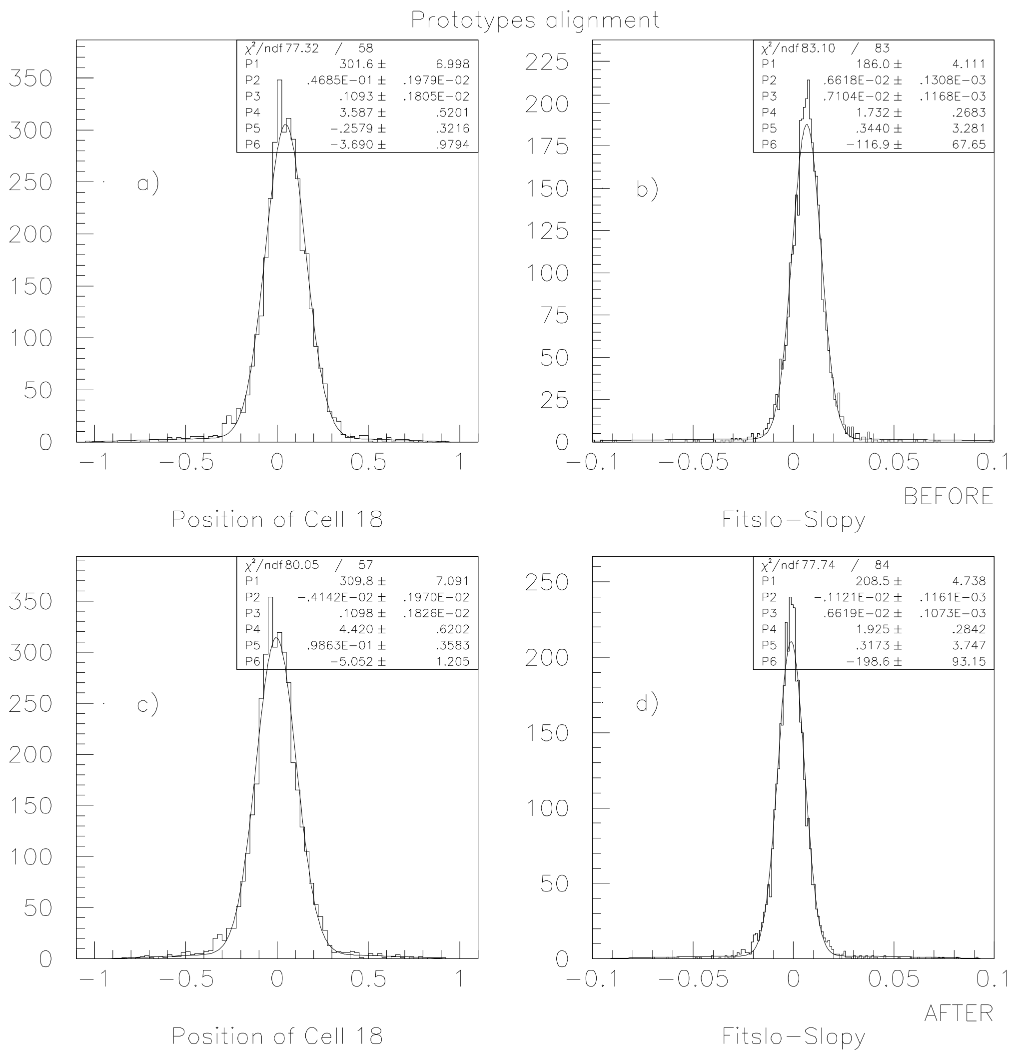

Figure 8. Plots showing the effect of the alignment procedure. a) Φ offset before corrections; b) Y displacement after the Φ correction; c),d) ΔY and $\Delta\Phi$ after corrections.

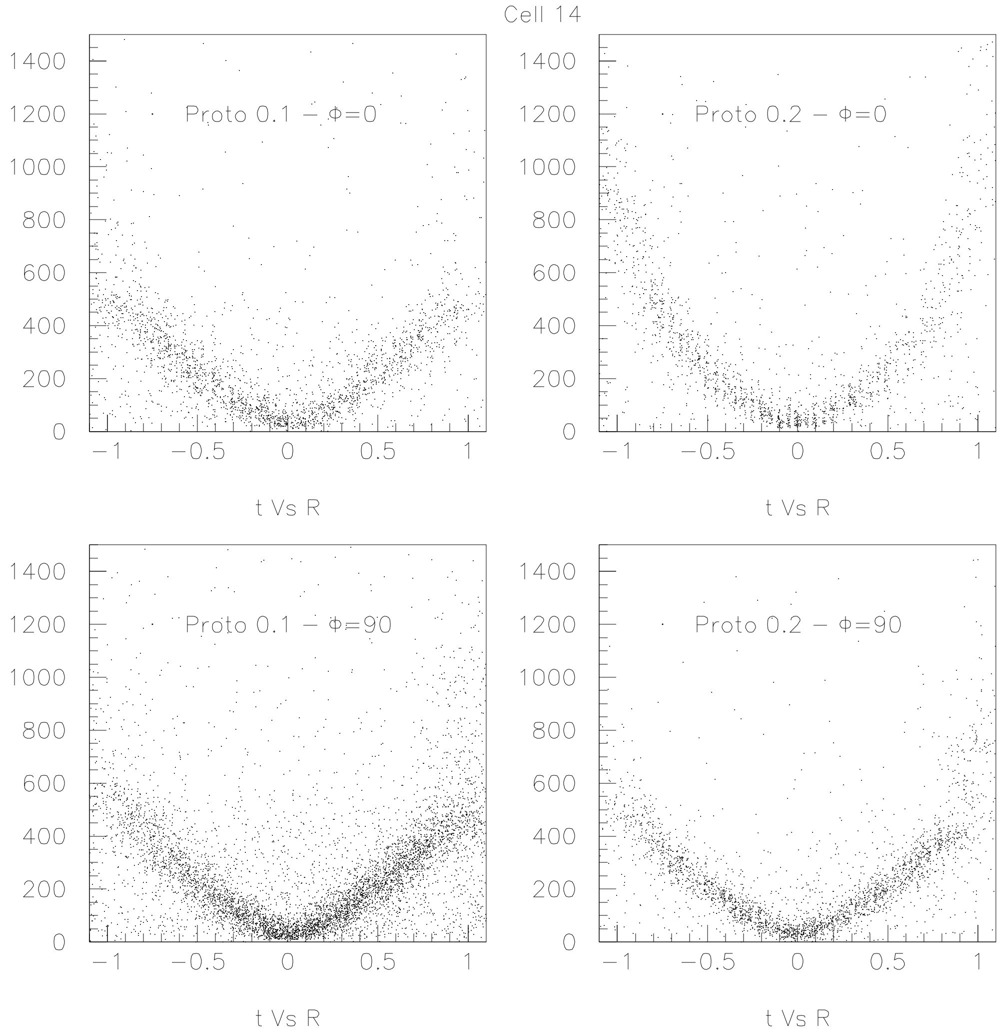

Figure 9. Plots showing the time-to-distance correlations.

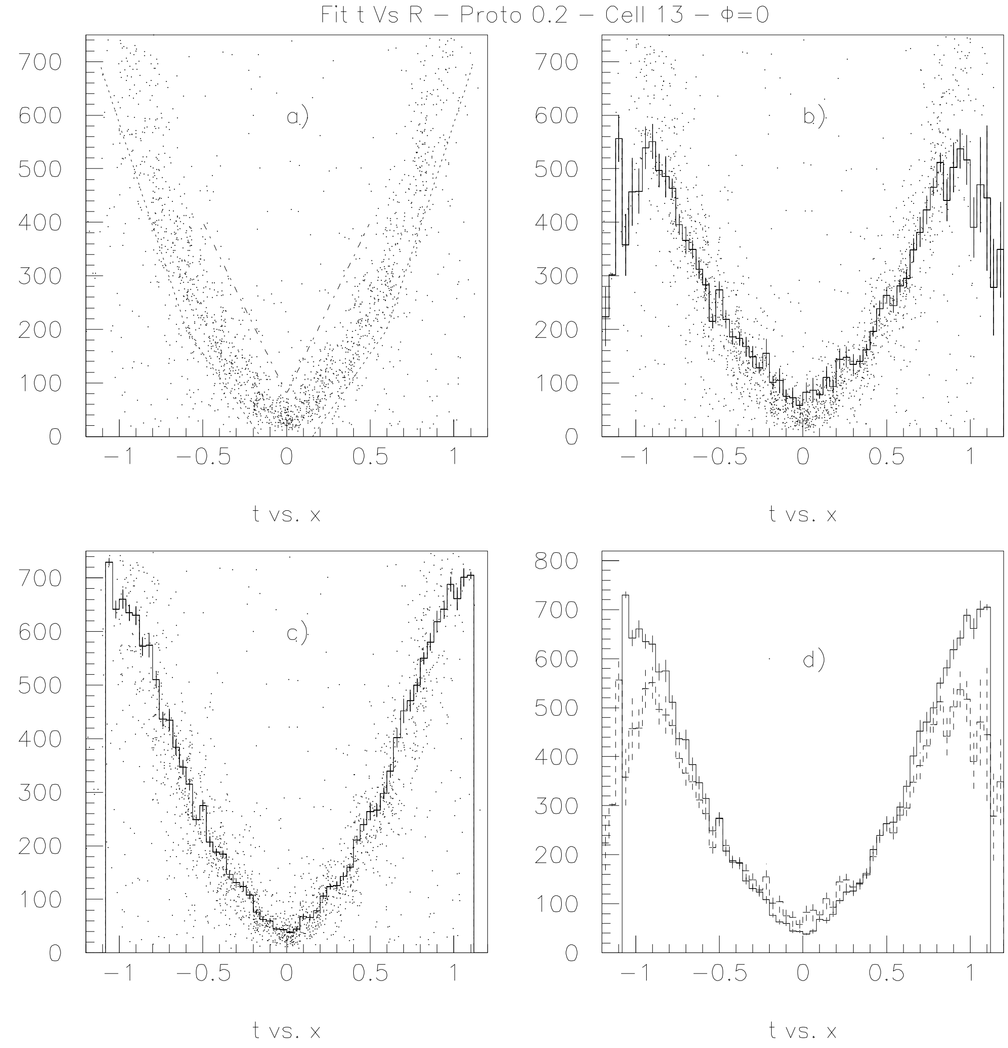

Figure 10. Fit of the time-to-distance correlation plots (see text).

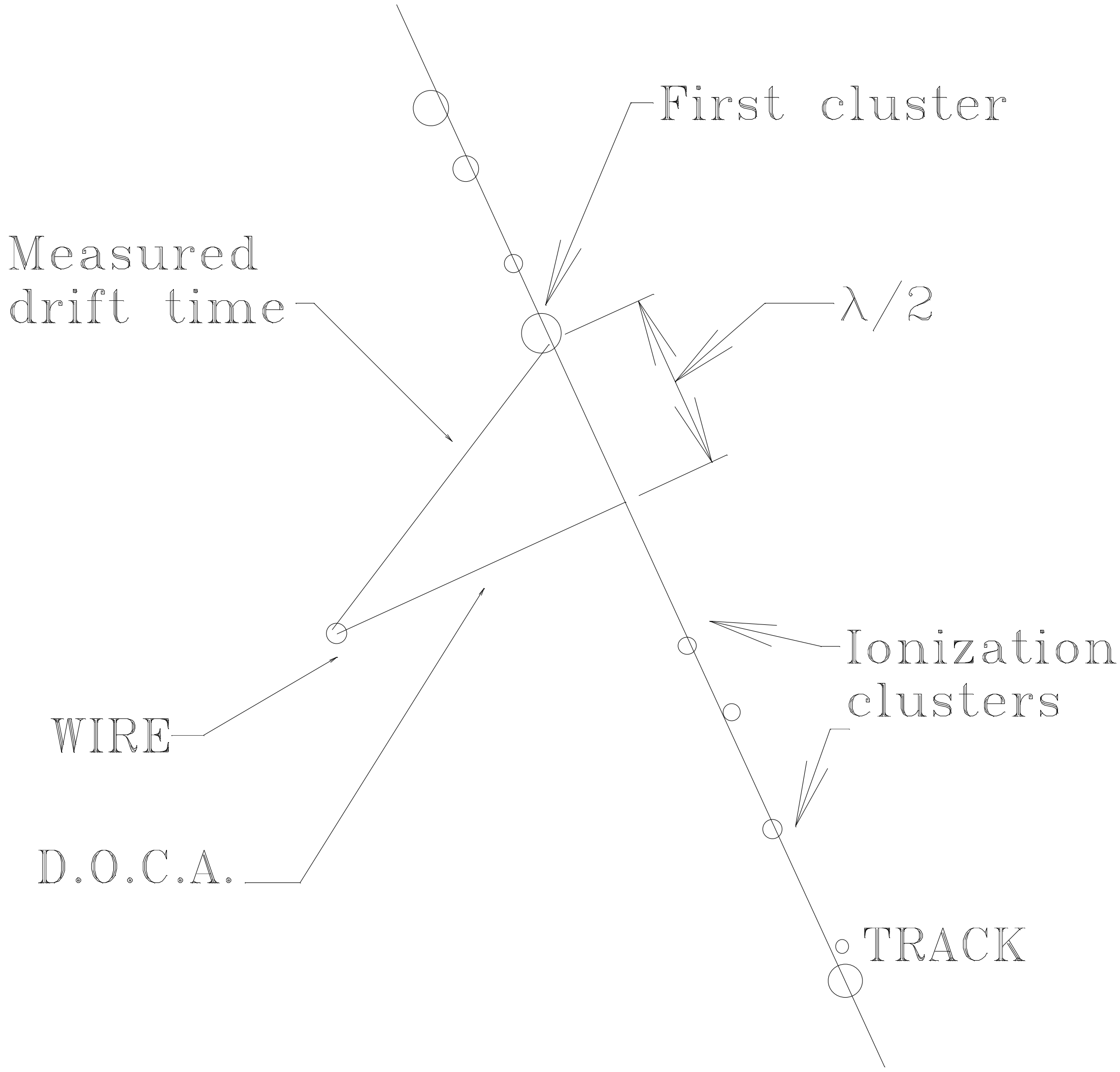

Figure 11. Effect of the ionization statistics on the time of arrival of the signal on the wires.

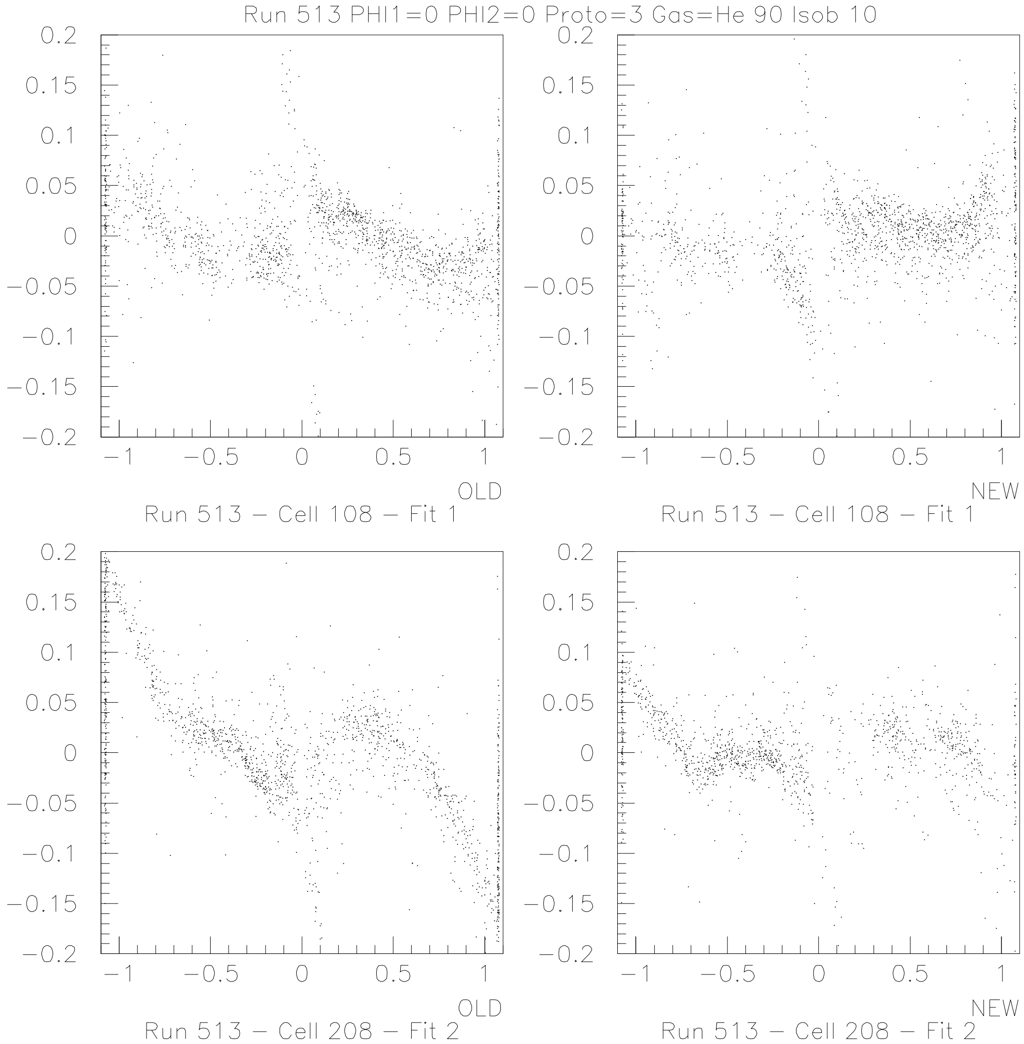

Figure 12. Comparison of the residuals as a function of R_d for the two fits, with t_0 fixed or fitted.

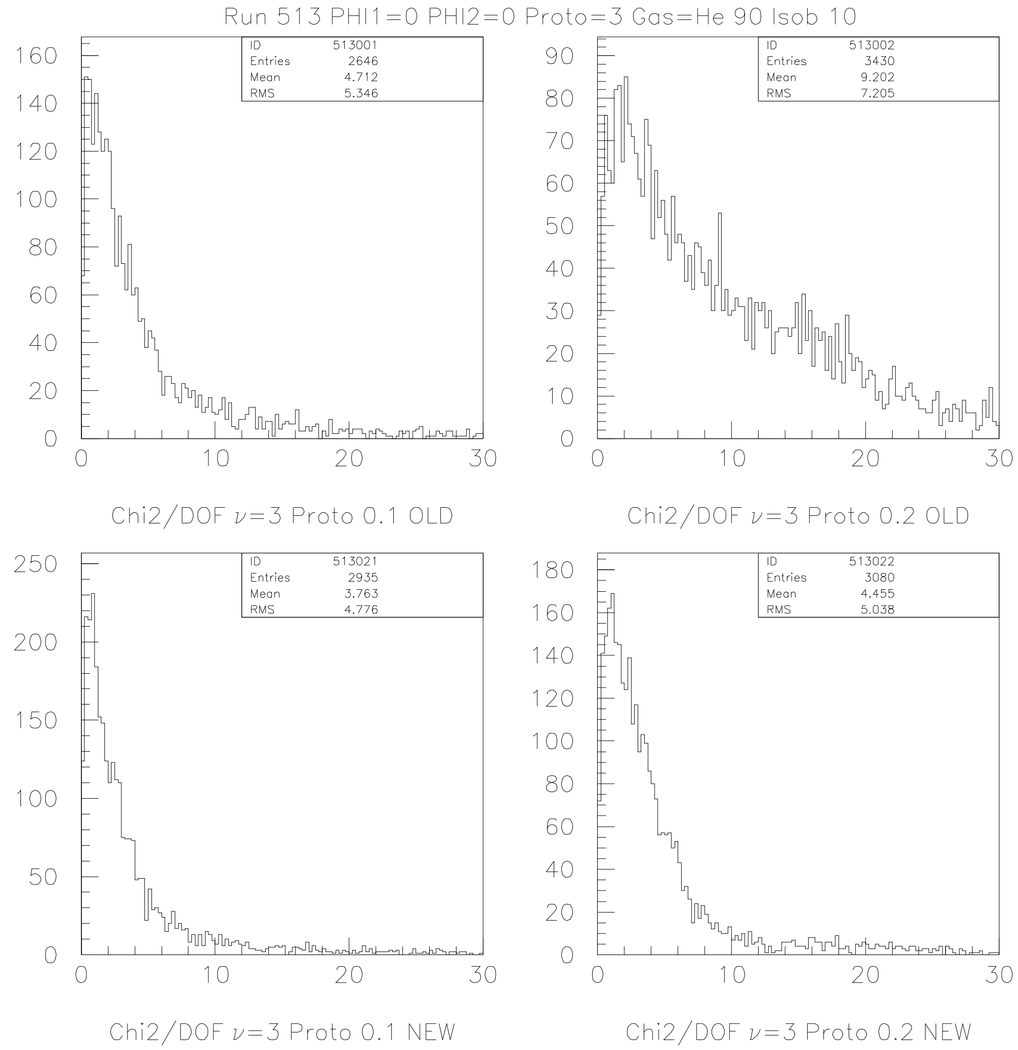

Figure 13. Comparison of the χ^2 for the two fits.

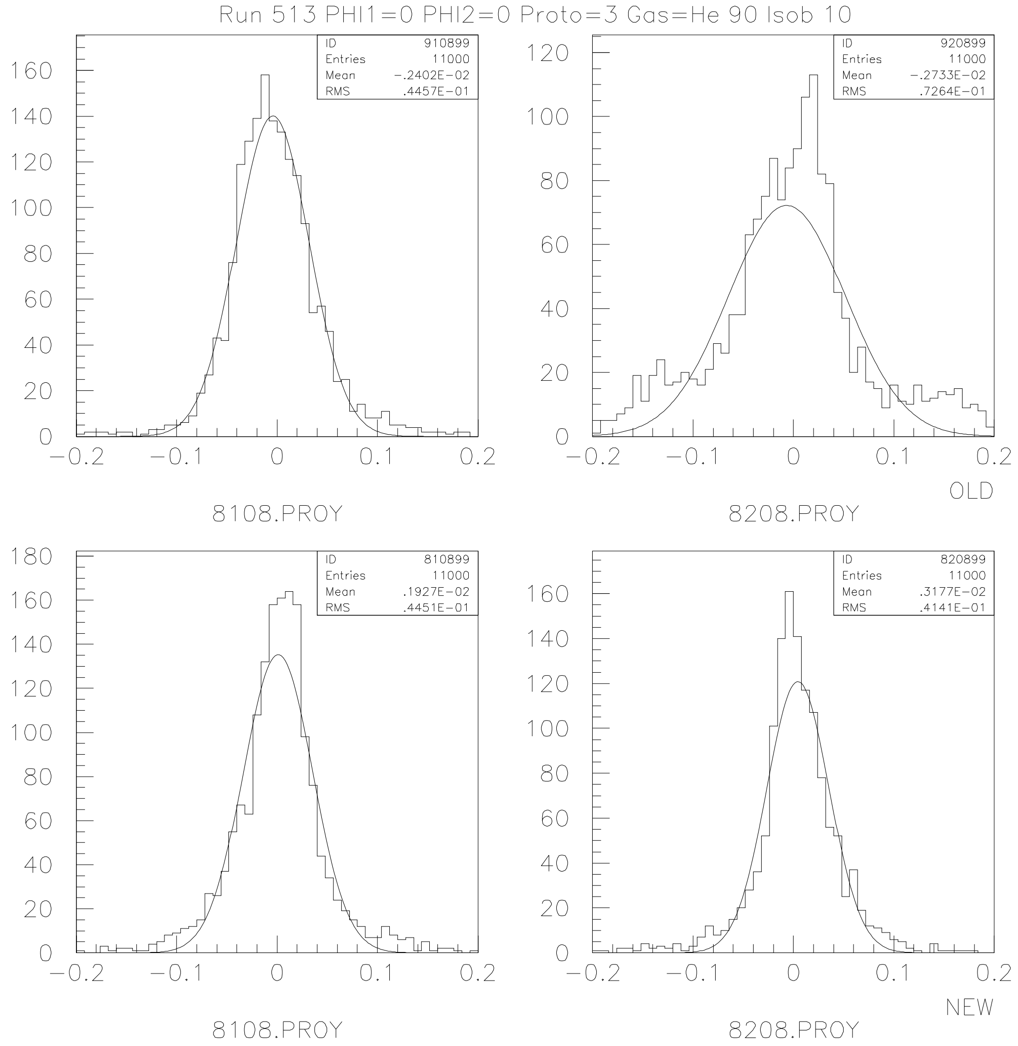

Figure 14. Comparison of the fit residuals averaged over the whole cell.

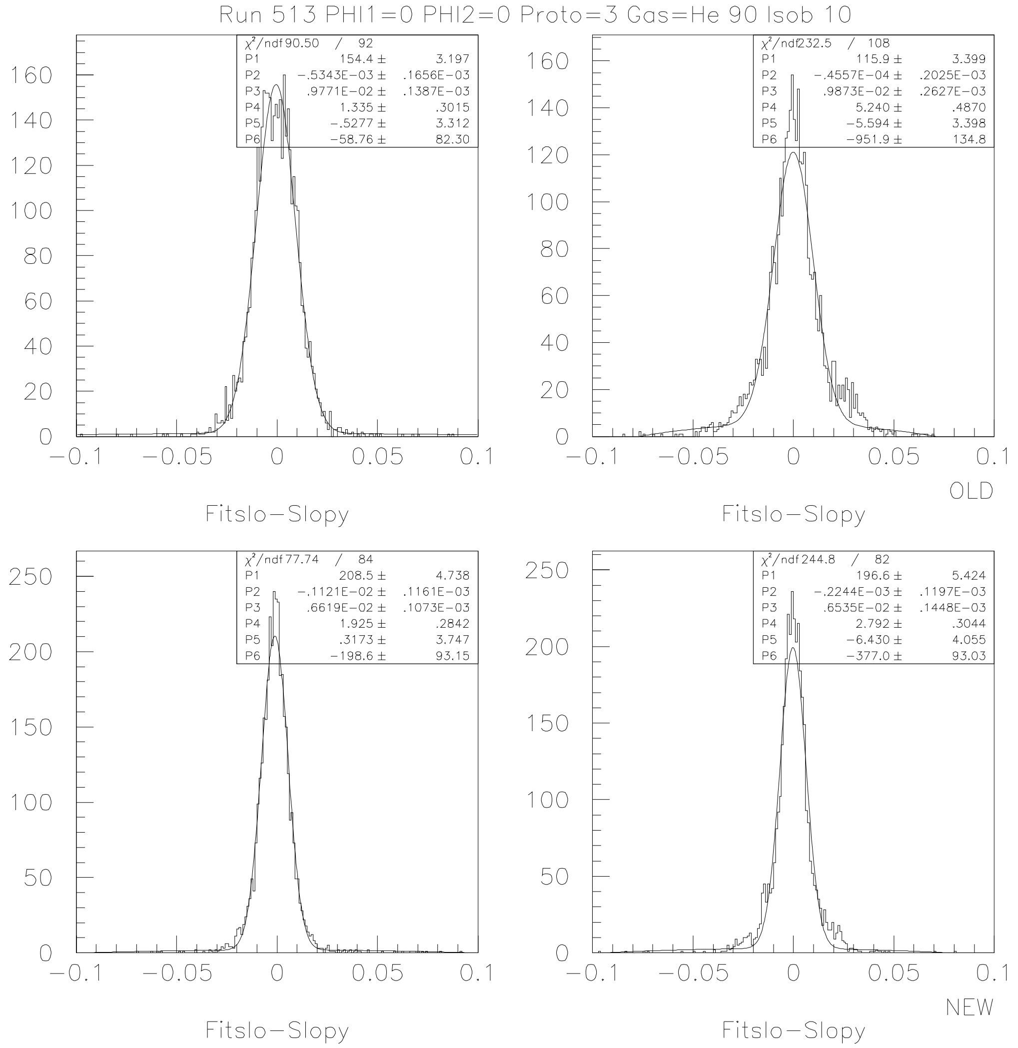

Figure 15. Comparison of the $\Delta\Phi$ distributions for the two fits.

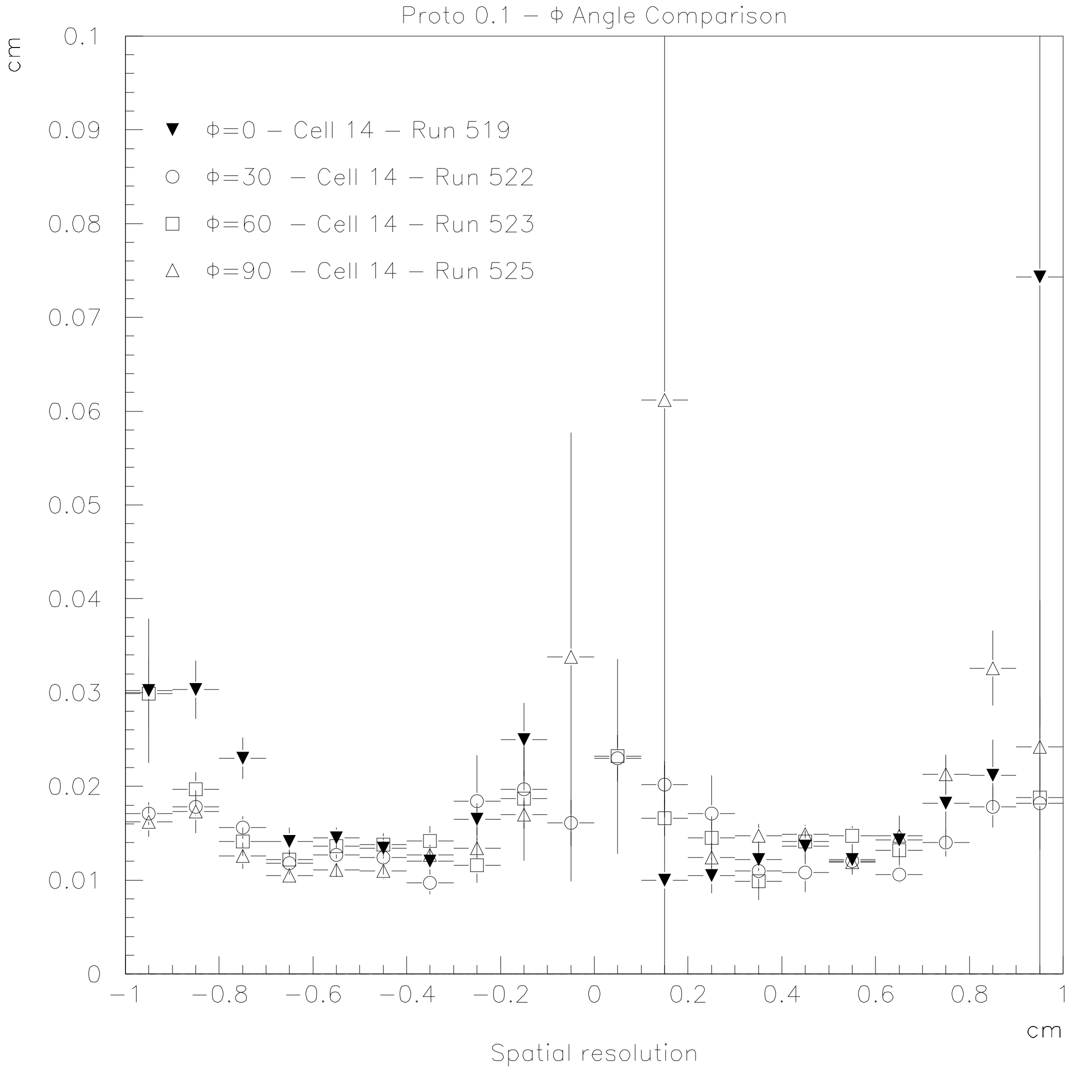

Figure 16. Fit residual as a function of R_d for different Φ angles in *Prototype 0.1* .

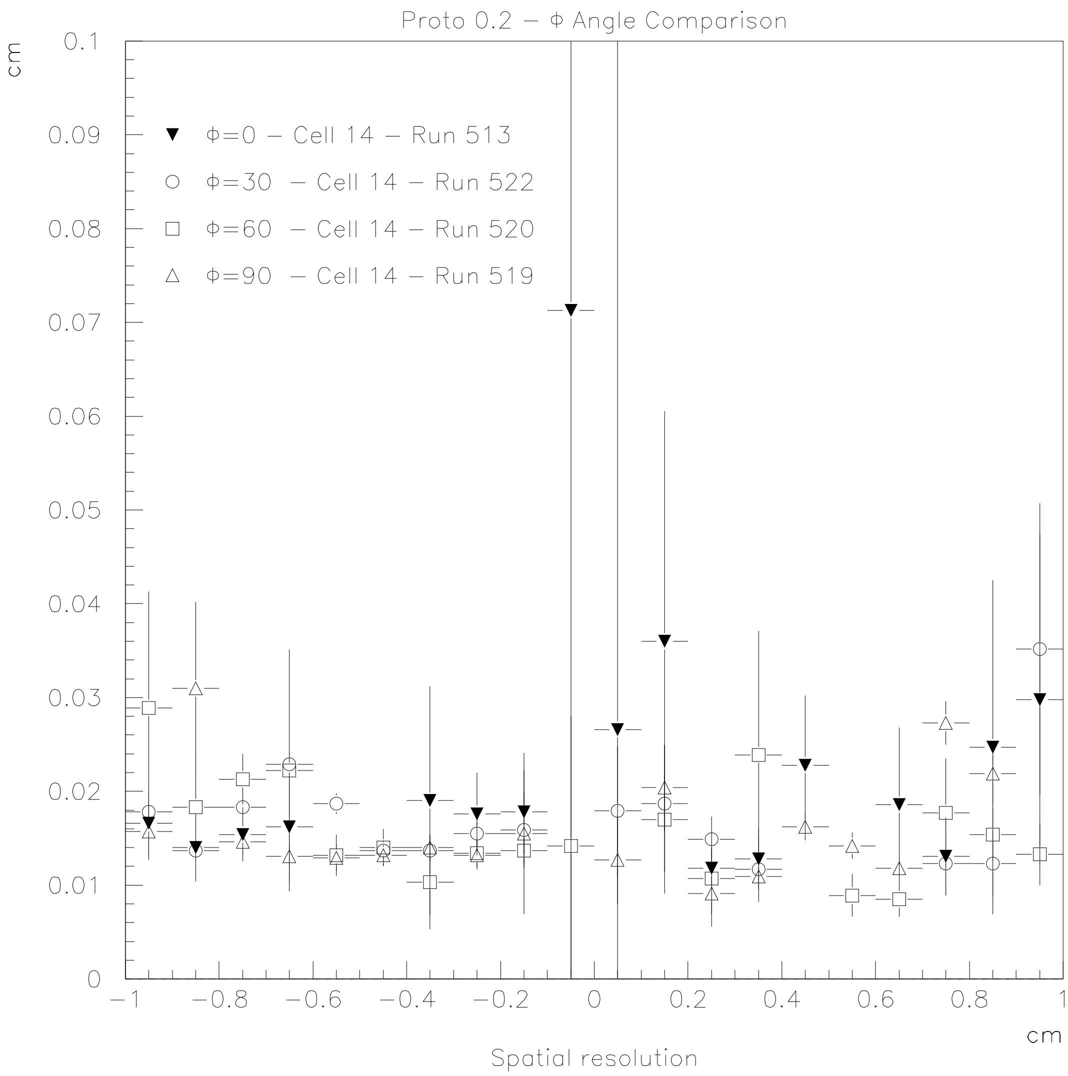

Figure 17. Fit residual as a function of R_d for different Φ angles in *Prototype 0.2* .

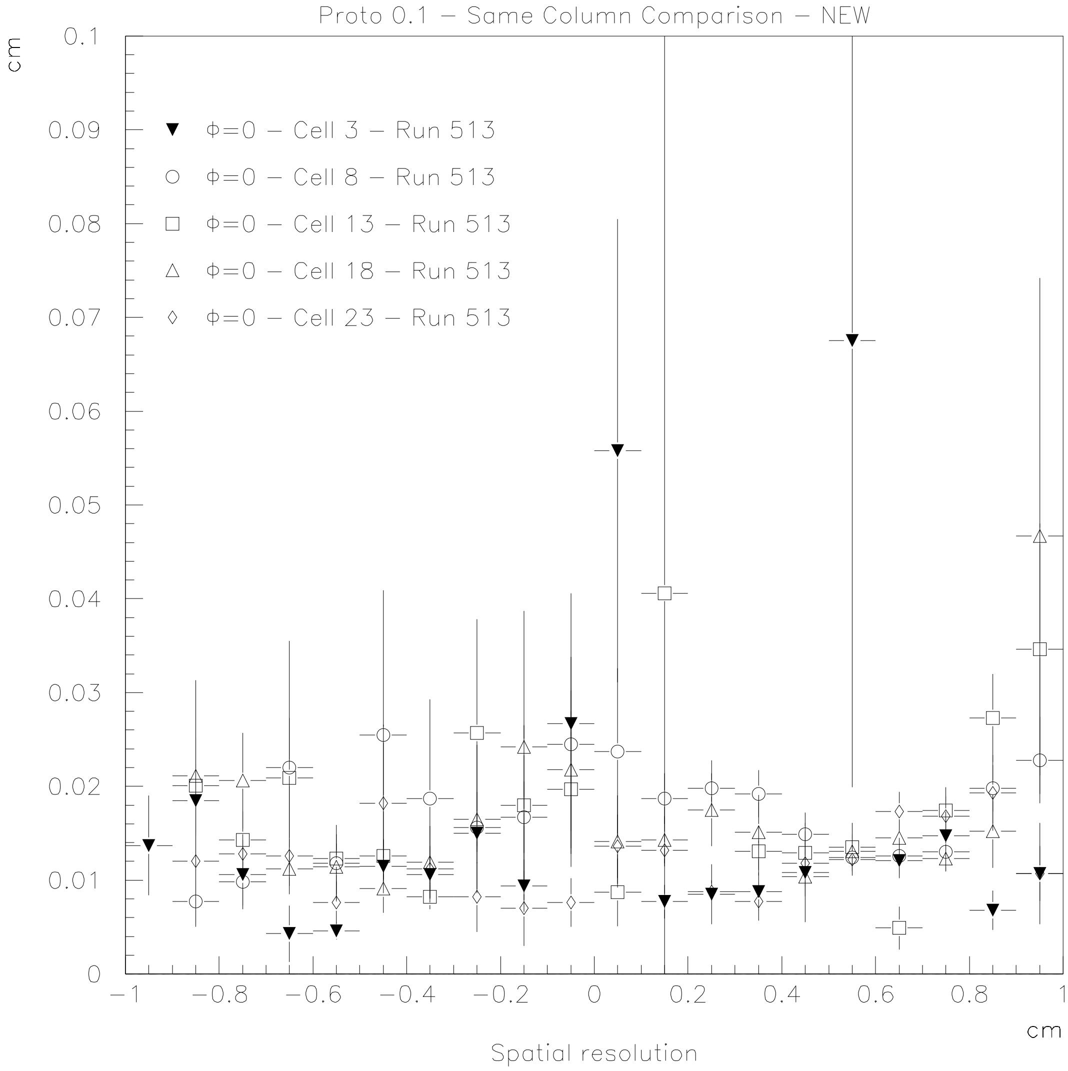

Figure 18. Fit residual as a function of R_d for different cells at the same Φ angle in *Prototype 0.1* .

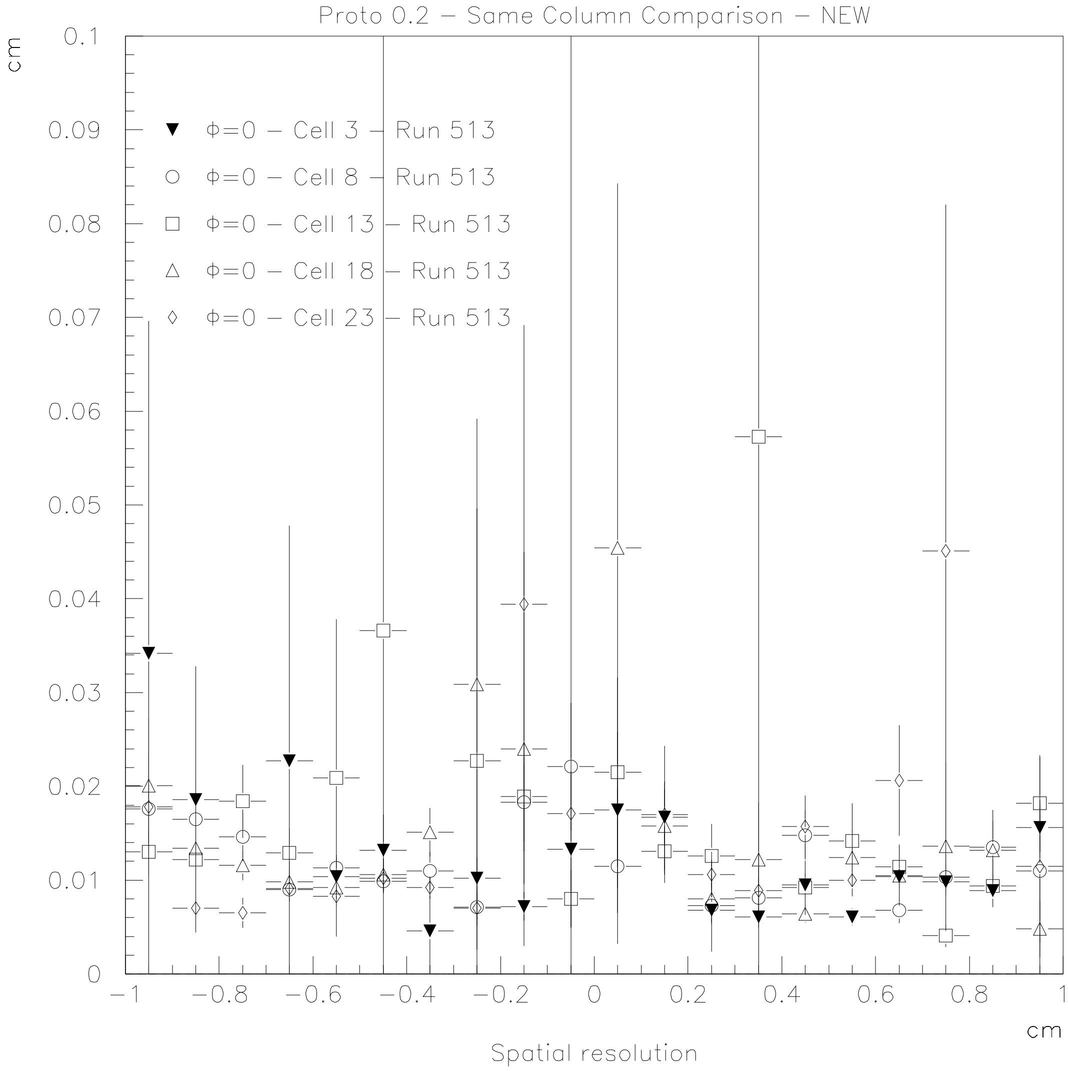

Figure 19. Fit residual as a function of R_d for different cells at the same Φ angle in *Prototype 0.2* .